Surfaces and Interfaces 75 (2025) 107817

Contents lists available at ScienceDirect

Surfaces and Interfaces

journal homepage: www.sciencedirect.com/journal/surfaces-and-interfaces

Does the oxidation degree of carbon nanofibers affect the friction and corrosion resistance of their reinforced PI resins?

Huiping Qi [a,b], Rui Yuan [a,b,*], Chang Tu [a,b], Hailian Bao [a,b], Zhaoyi Zhu [a,b], Zhili Chen [a,b], Jing Yuan [c]

[a] Salt Lake Chemical Engineering Research Complex, College of Chemical Engineering, Qinghai University, Xining 810016, China
[b] Collaborative Innovation Center of Chemistry and Process Engineering for Salt Lake Resource, Qinghai University, Xining 810016, China
[c] Qinghai Provincial Key Laboratory of Nanomaterials and Technology, Qinghai Minzu University, Xining, Qinghai 810007, China

ARTICLE INFO

Keywords:
Carbon nanofibers
Oxidation degree
Polyimide
Friction and wear properties
Corrosion resistance
MD simulation

ABSTRACT

Oxidation treatment was usually a prerequisite step of carbon nanofibers (CNFs) functionalized modification. However, does different oxidation process affect CNFs reinforcement properties? To address this question, we prepared CNFs with different oxidation degrees by controlling the frequency of ultrasound, labelled as CNF-1 (4 kHz), CNF-2 (20 kHz) and CNF-3 (40 kHz), and further investigated the effects of different CNFs on the friction properties and corrosion resistance of polyimide (PI). The friction results showed that the coefficients of friction of PI, CNF/PI, CNF-1/PI, CNF-2/PI and CNF-3/PI were 0.3594, 0.3077, 0.3059, 0.2991 and 0.2643 (0.5 wt%), and their wear rates were PI>CNF/PI>CNF-1/PI>CNF-2/PI>CNF-3/PI, further confirming that the incorporation of CNFs enhances the frictional properties of the PI coating by increasing the mechanical strength. In addition, oxidation led to a better compatibility of the CNFs with the PI chains and obvious enhancement effect. However, different results were obtained in terms of corrosion resistance, with only the CNF-3/PI (2.8×10^{-7} A/cm^2) coating having a lower corrosion current density than pure PI (4.0×10^{-7} A/cm^2). MD simulation further revealed the mechanism of CNF and oxidized CNF on the corrosion resistance of PI resin by investigating the interaction between CNF/ oxidized CNF with PI chains and the diffusion behaviors of NaCl-H_2O. It was found that the poor compatibility of CNFs with PI chains and their vertical arrangement were detrimental to the corrosion resistance of the resin. Therefore, high dispersion of the nanofillers and good compatibility with the resin became even more critical in the corrosive environment.

1. Introduction

Wear and corrosion are prevalent in nature and in engineering practice and can cause significant energy loss and economic damage. According to statistics, 30 %-50 % of global energy loss is caused by friction, and about 80 % of cases of mechanical failure are caused by wear and tear[1,2]. Polyimide (PI) is a common polymer lubrication corrosion protection material [3,4]. As early as the 1970s, NASA discovered that the coefficient of friction of PI could be as low as 0.1[5]. However, under certain extreme operating conditions, pure PI is unable to maintain a low coefficient of friction and a low wear rate. Its corrosion resistance is also inconsistent, making it difficult to meet application requirements. Research and practice have shown that incorporating reinforcing fibers, solid lubricants and functional nanofillers into PI resins can significantly enhance both the tribological properties and corrosion resistance of coatings [6–9].

Carbon nanofibers (CNFs) are one-dimensional nanomaterials characterized by high strength, high modulus, resistance to friction and corrosion, as well as good thermal stability. These properties make them excellent reinforcement materials [10–12]. Cho et al. investigated the tribological properties of carbon fibers reinforced polyphenylene sulfide and found that the coefficient of friction of PPS+CF was reduced to 0.2-0.3, and this is because a smooth layer of carbon forms on the surface of the stainless steel when it slides[13]. Wu et al. used MoS_2-functionalized CNFs as a reinforcing filler for epoxy resin, and the tensile strength of the resin was increased by 56.6%, and its corrosion current density of the composite coatings was also reduced from 1.04×10^{-6} A cm^{-2} to 6.76×10^{-8} A cm^{-2}[14]. Zhu et al. discovered that CNFs when modified with n-octadecane could effectively improve the mechanical strength and abrasion resistance of PI resins, increasing their

* Correspondence author.
E-mail address: yuanruiqhdx@163.com (R. Yuan).

https://doi.org/10.1016/j.surfin.2025.107817
Received 7 June 2025; Received in revised form 1 September 2025; Accepted 7 October 2025
Available online 8 October 2025

elongation-to-break, tensile strength, bending strength and impact strength by 150 %, 29.4 %, 26.7 % and 183 %[15]. In addition to enhancing the friction and wear properties of the resins, CNFs also effective in improving its corrosion resistance. A.R. Siddiqui et al. designed a corrosion-resistant, self-cleaning and superhydrophobic CNFs coating using its entangled forms[16]. Fatma et al. prepared a CNF-doped polydimethylsiloxane (PDMS) corrosion-resistant composite (CNF-PDMS) and coated them on the anode material, achieving a reduction in corrosion rate from (17±6) × 10^3 μm y^{-1} to 93±23 μm y^{-1}[17]. Zhao et al. polymerized a layer of polyaniline in situ on the surface of CNFs and added it to an aqueous epoxy resin, which effectively improved the corrosion resistance of the coating. Compared to polyaniline coatings, the corrosion potential increased by 157%, while the corrosion current density decreased by 78% [18]. However, unmodified CNFs have a smooth surface, lack sufficient polar functional groups, and exhibit low surface activity, leading to poor wettability with the resin matrix. This results in weak interfacial bonding in the reinforced composites, preventing the excellent properties of CNFs from being fully utilized. Therefore, the surface modification of CNFs is required before introducing them into the resin[19–22]. However, most research has focused on the functionalization of CNFs surfaces using different modifying groups, which is often preceded by an oxidation treatment. In fact, the functionalized modified grafting rate of CNFs is relatively limited. Thus, the pre-oxidation treatment significantly influences the surface properties and enhancement properties of CNFs that it is often neglected[23,24]. Therefore, several questions need to be explored: How much does the degree of oxidation affect the reinforcing properties of CNFs? What is the difference in the reinforcement mechanism of CNFs as a nanofiller in improving the friction and wear performance and corrosion resistance of PI resins?

To address the above questions, we prepared CNFs with different degrees of oxidation by adjusting the ultrasound frequency, CNF-1, CNF-2 and CNF-3. These CNFs were added into the PI resin to investigate the effect of CNFs with different oxidation degree on the friction and wear performance, as well as the corrosion resistance of the resin. Our study provides technical guidance for the oxidation treatment of CNFs.

2. Experimental section

2.1. Materials

CNFs were commercially obtained from Shanghai Aladdin Biochemical Technology Co. Ltd. (Shanghai, China). PI resin was obtained from Beijing Huatong Ruichi Material Technology Co. Ltd. (Beijing, China). N methyl pyrrolidone was purchased from Anhui Zesheng Technology Co. Ltd. (Anhui, China). Concentrated sulfuric acid, concentrated nitric acid, hydrogen peroxide and potassium permanganate were obtained from Sinopharm Chemical Reagent Co. Ltd. (Shanghai, China).

2.2. Preparation

Preparation of CNFs with different degrees of oxidation: CNFs (2 g) and potassium permanganate (4.5 g) were slowly added to a mixed acid solution (concentrated sulfuric cid: concentrated nitric acid = 9:1). The mixture was warmed up to 50°C and placed in a sonication apparatus at different ultrasonic frequencies for 2 h. After sonication 200 mL, 30 % hydrogen peroxide solution was added and stirred for 0.5 h. The mixture was centrifuged, the supernatant was decanted to remove the sediment, washed with plenty of water until the pH was neutral. The obtained products were dried in an oven at 80°C and labeled according to the ultrasonic frequency during oxidation as CNF-1 (4 kHz), CNF-2 (20 kHz), and CNF-3 (40 kHz).

Preparation of CNF-based/PI coatings: Disperse CNFs with varying oxidation levels in N methyl pyrrolidone and sonicate for 0.5 h to ensure thorough dispersion. Slowly add the mixture dropwise to mechanically stirred PI prepolymer (65% solids), stir thoroughly, then pour the mixture into a spray gun for coating the film. Before spraying, the working surface of the steel substrate was sanded by coarse sandpaper to increase the bonding of the resin to the steel block and cleaned with anhydrous ethanol. The PI-based mixture was sprayed onto the pretreated steel blocks using a spray gun (RG-3L, ANEST IWATA Corporation, Japan) at 0.2 MPa under high-purity nitrogen gas, followed by curing. Curing was performed in two stages. First, the steel block was cured in an oven at 120°C for 2 h to remove most of the solvent. Subsequently, the temperature was raised to 220°C, and curing continued for 2 h to ensure complete solvent removal. The process of oxidizing CNFs and preparing PI-based composite coatings was shown in Fig. 1.

2.3. Characterizations

The morphology and structure were observed using field emission scanning electron microscopy (FE-SEM, JSM-7900F, Japan, Acceleration Voltage: 5 kV) and transmission electron microscopy (TEM, Grand ARMII Spectra 300, USA). An x-ray photoelectron spectrometer (XPS, ESCALAB, Thermo Fisher, USA), x-ray electron diffraction (XRD, D-max2500PC Rigaku, Japan), Laser confocal Raman microscope (InVia Qontor, Renishaw, UK; laser wavelength: 532 nm; exposure time: 1 s; laser power: 5%; accumulation: 1) measured Raman spectra and Fourier infrared (FT-IR, Nicolet 6700, USA) to analyze the surface composition of CNFs-based fillers. In Raman spectroscopy, the calculation of D and G peak intensities employs the peak area integration method.

The friction and wear testing of the coating was conducted using an MS-T3001 friction tester (China Lanzhou Huahui Instrument Technology Co., Ltd.). In the experiment, a stainless-steel ball (GCr15 material, diameter 5 mm, surface roughness Ra=20 nm, hardness 66 HRC) was employed to perform rotational friction on the coating surface. The applied load was 3 N, the rotational speed was set to 300 r/min and the duration was 2 h. All friction tests on the coatings were conducted at room temperature (approximately 25°C) and humidity (approximately 32%). The surface morphology of the grinding balls was examined using an optical microscope (InVia Qontor, Renishaw, UK) and a 3D profilometer (SuperView W1 CHOTEST, China). The grinding debris was characterized by field emission scanning electron microscope (SEM, JSM-7900F, Japan, acceleration voltage: 10 kV). The surface morphology and roughness of the coating were investigated using atomic force microscope (AFM, Dimension ICON, Bruker Corporation, USA, ScanAsyst mode) and a 3D profilometer (SuperView W1 CHOTEST, China). Morphology of coating wear marks were investigated by scanning electron microscope (SEM, JSM-6610LV, Japan, acceleration voltage: 10 kV). The coating hardness was measured by nanoindentation scratch tester (STeP 500, CH, maximum load: 25 mN, dwell time: 10 s).

The corrosion performance of the coating was investigated using an electrochemical workstation (CHI760E, China) and a flat-plate corrosion test cell (C010, Wuhan Gaoshiruilian Technology Co., Ltd.). The reference electrode is an Ag/AgCl electrode, the counter electrode is a platinum electrode, and the working electrode is the sample. The corrosion medium used in this experiment is a 3.5 wt% aqueous solution of NaCl. The polarization curves were scanned at a rate of 0.01 V/s. The corrosion potential (E_{corr}) and the corrosion current density (I_{corr}) were obtained by fitting a linear extrapolation of the polarization curves.

2.4. Computational analysis

The morphology and corrosion resistance of PI, CNF/PI and Oxidized CNF /PI were investigated using molecular simulations[25]. Due to the limitation of the simulation computing equipment, the simulation of the actual carbon fiber cannot be realized. Therefore, a single-arm carbon nanotube with diameter 7.49 Å and length 30.61 Å was selected as a substitute carbon fiber and labeled as CNF (Fig. 2a). Further, oxygen-containing functional groups, hydroxyl (6), epoxy (2), carboxyl (4) and carbonyl (4) were introduced on the surface of CNF and labeled

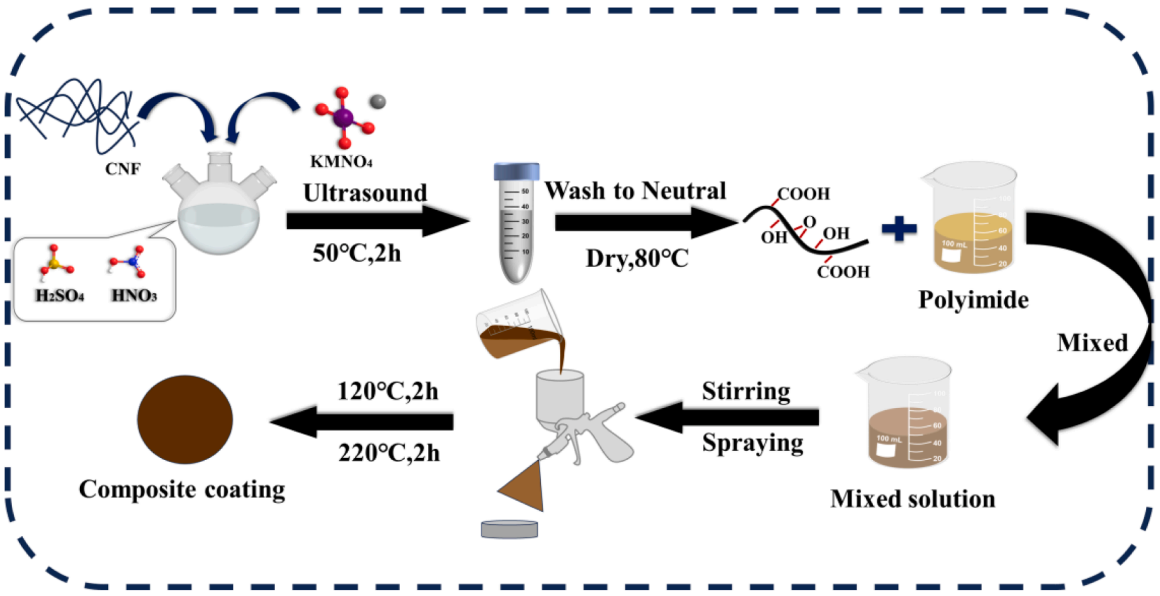

Fig. 1. Preparation of CNFs-based composite fillers and PI-based coatings.

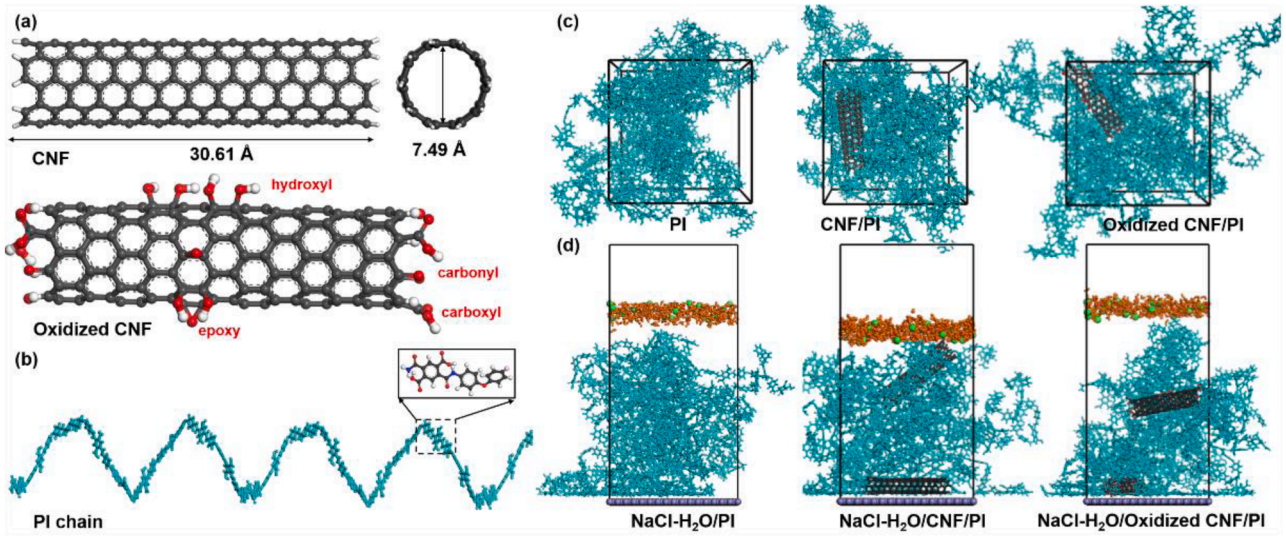

Fig. 2. Schematic diagram of CNF, oxidized CNF (a), PI chains (b), pure PI, CNF/PI, oxidized CNF/PI (c), NaCl-H_2O/PI, NaCl-H_2O/CNF/PI and NaCl-H_2O/oxidized CNF /PI (d).
(PI chains are cyan; H_2O are orange, and Cl^- are green).

as Oxidized CNF [26]. PI chain consisted of 20 monomers with isotropic homo-polymerization (Fig.2b). For PI-based system, the added PI chain and CNF are 20 and 1. The PI, CNF/PI and Oxidized CNF /PI systems were further constructed (Fig.2c). To investigate the corrosion resistance mechanism, a model was constructed with an Fe substrate at the bottom, a PI coating on top of it, and the NaCl-H_2O system above the coating, increasing the CNF and oxidized CNF content in the system by two, as shown in Fig. 2d. Among them, the Fe substrate was selected as the Fe (1 0 0) metal surface. The NaCl-H_2O was consisted of H_2O (400), Cl^-(20) and Na^+(20).

The interatomic interaction in PI-based systems was described by the Condensed-phase Optimized Molecular Potentials for Atomistic Simulation Studies (COMPASS) force field[27]. The temperature of the systems was controlled by the Nose thermostat[28]. All constructed initial models were structurally optimized by Smart algorithm, followed by the thermal annealing process, and the satisfying the equilibrium using the constant-temperature and pressure ensemble (NPT, 298 K, 0 GPa, 0.5 ns, 1.0 fs) and the constant-temperature and volume ensemble (NVT, 298 K, 1.0 ns, 1.0 fs)[29]. For corrosion processes, the NVT dynamics were run for 3 ns (1.0 fs).

3. Results and discussion

3.1. Characterization of the CNF-based fillers

Fig. 3(a-d) showed the morphologies of CNF, CNF-1, CNF-2 and CNF-3. CNF presented a cylindrical tubular structure with a diameter of about 280 nm and a relatively smooth surface. However, the surface of CNF-1, CNF-2 and CNF-3 after oxidization treatment showed more serious damage, and even the morphology gradually changed from tubular to filamentary multilayered structure (I, II, III)[19,23]. From the EDS results, the content of oxygen atoms on CNFs increased significantly after oxidization, as shown by the uniform distribution of C and O elements in CNF-1, CNF-2 and CNF-3. In addition, the oxidation treatment also

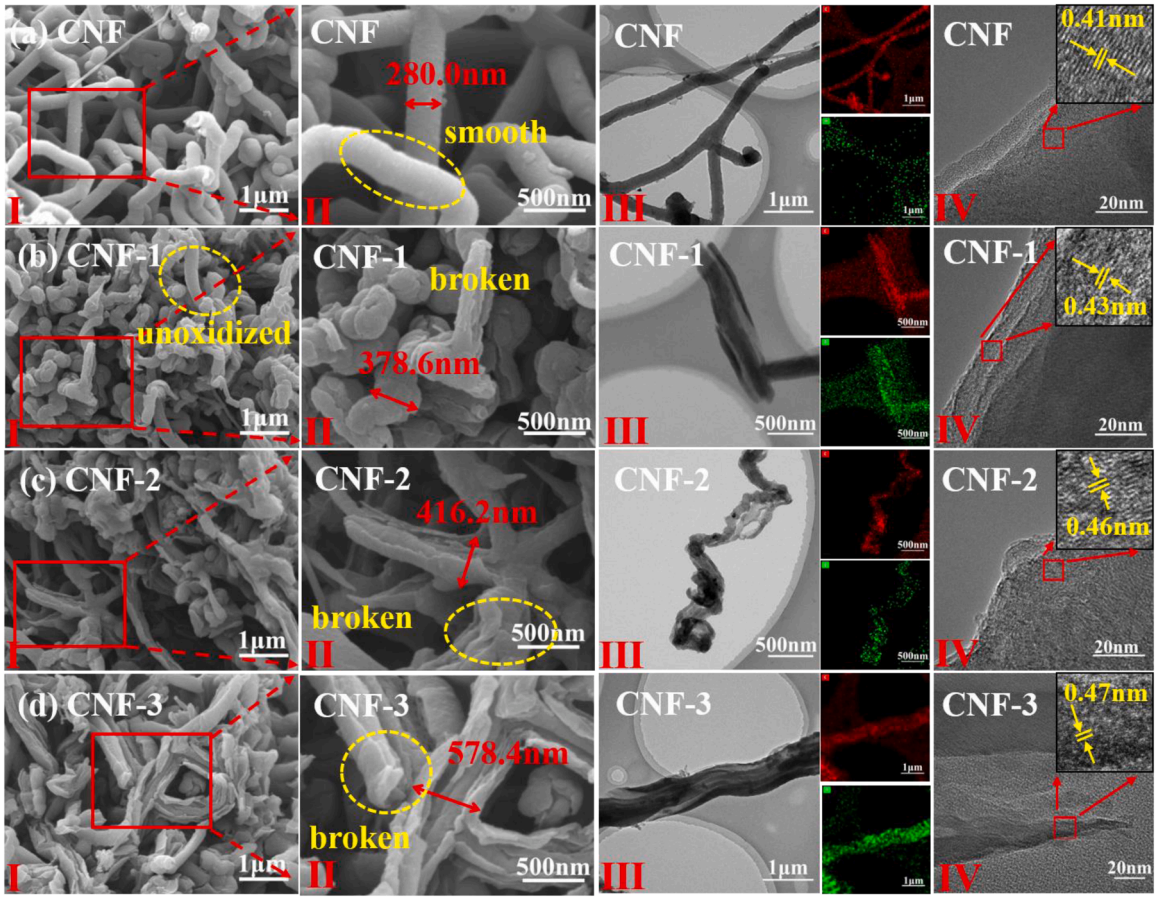

Fig. 3. FE-SEM (I, II), TEM (III), HRTEM (IV) and the corresponding EDS maps of CNF(a), CNF-1(b), CNF-2(c) and CNF-3(d).

disrupted the regular structure of CNFs. By introducing oxygen atoms between the layers, the CNF layer spacing was increased from 0.41 nm to 0.47 nm(IV).

Based on this, the effects of oxidation treatment on CNFs have three main aspects: firstly, oxidation treatment destroys the regular structure of CNFs, resulting in a decrease in their mechanical properties; secondly, oxidation treatment introduces oxygen-containing functional groups on the surface of CNFs which can increase the bonding force between them and the resin; thirdly, more internal lamellae are exposed after the oxidation, which also increases the contact area of the CNFs with the resin. Therefore, the oxidation treatment is to improve the resin bonding of CNFs on the basis of depletion of their mechanical strength.

The degree of oxidation of CNFs was further investigated using XPS. The ratio of C and O atoms (C/O) in CNFs varied with the degree of oxidation of CNFs (Fig.4a). With the increase of ultrasound frequency, the value of C/O decreased from 5.50 (CNF) to 0.65 (CNF-3), which indicated that oxygen atoms were successfully grafted on the CNFs, and further verified that it was feasible to achieve the preparation of CNFs with different oxidation degree by controlled ultrasound (Fig. 4b). The C1s of CNFs were deconvoluted into peaks at 284.6 eV (C-C), 286.1 eV (C-OH), 286.8 eV (C-O-C), 287.7 eV (C=O) and 289.0 eV (COOH) (Fig.4c-f)[30–32]. From CNF to CNF-3, the C-OH, C-O-C, C=O and COOH increased by 7.9 %, 8.9 %, 11.5 % and 4.8 % respectively. Furthermore, the corresponding data on oxygen-containing functional group content are presented in Table 1. This suggested that controlling the frequency of ultrasound favored the grafting of C=O groups, while COOH groups were less grafted. The chemical composition of CNFs was further investigated by FTIR (Fig. 4g). The stretching vibration peaks of surface functional groups on CNFs were observed at 1230cm^{-1}(C-O/-C-O-C), 1630cm^{-1}(C=C), 1730 cm^{-1}(C=O) and 3421cm^{-1}(-OH/COOH), where CNF-1, CNF-2, and CNF-3 in which the C-O/C-O-C and C=O vibrations were more prominent, indicating an increased abundance of oxygen-containing functional groups on the CNFs surface, confirming the occurrence of surface oxidation [33,34].

In the Raman spectrum, the D and G peaks were located at 1350 cm^{-1}and 1583 cm^{-1}, and the intensity ratio of the D and G peaks is used to assess carbon defects and amorphous carbon content (Fig. 4h). It has been shown that oxidation destroys the sp^2 hybridized structure of carbon, thereby increasing the defect density and at the same time increasing the amorphous carbon content[23,31,32]. From CNF to CNF-3, the values of $I_{(D)}/I_{(G)}$ were 0.98, 1.15, 1.20 and 1.44. Therefore, increasing the frequency of ultrasound could enhance the degree of CNFs oxidation. The information related to the structure of the samples analyzed using XRD was shown in Fig. 4i, and the diffraction peaks of CNF, CNF-1, CNF-2 and CNF-3 were located at 25.78° (3.46 Å), 25.68° (3.47 Å), 25.62°(3.48 Å) and 25.56°(3.49 Å) and the diffraction peaks were shifted to the left compared to CNFs, which might be due to the introduction of oxygen-containing groups, which increased the CNFs cell parameters and increased the crystal plane spacing [35–37]. Therefore, it was feasible to change the degree of oxidation of CNFs by controlling the ultrasound frequency.

3.2. *Surface morphology and hardness of CNF/PI coating*

Fig. 5(a-e) showed the surface morphology of coatings. The PI coating was smoother and the rest of the coatings had small particles of bumps on the surface, which was caused by the mixed CNFs (I). The surface roughness was measured by 3D profilometer as 142 nm, 206 nm, 212 nm, 201 nm and 172 nm (II). Similar results were obtained by AFM measurements its surface roughness was 2.36 nm, 3.59 nm, 4.83 nm,

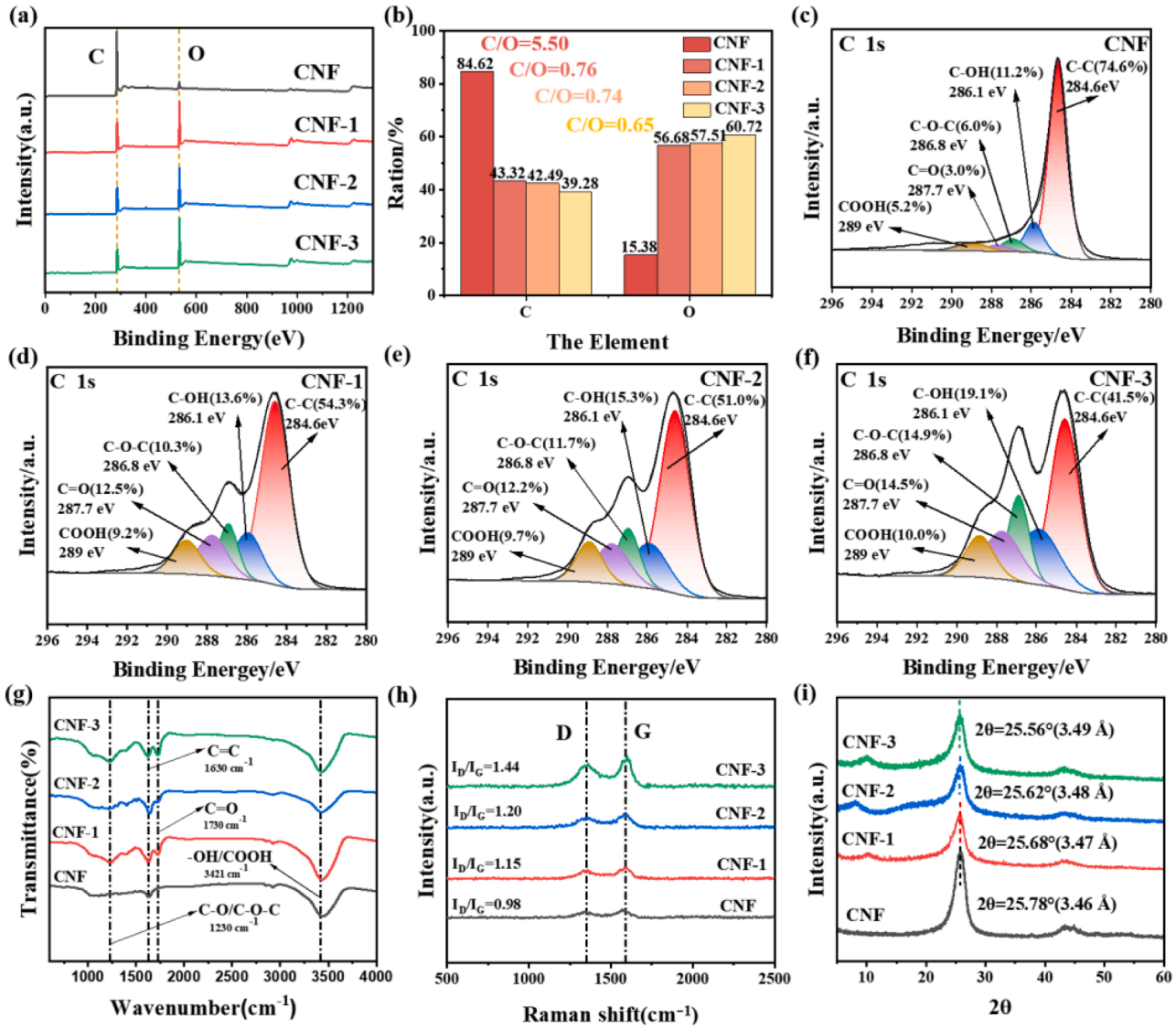

Fig. 4. Chemical property of the CNF, CNF-1, CNF-2 and CNF-3 (a-b) XPS survey and Content of C and O elements, (c-f) XPS C1s spectra and (g-i) FTIR, Raman and XRD patterns.

Table 1
Oxygen-containing functional group content (%) of CNF, CNF-1, CNF-2 and CNF-3.

System	Oxygen-containing functional group content (%)				
	C-C	C-OH	C-O-C	C=O	COOH
CNF	74.6	11.2	6.0	3.0	5.2
CNF-1	54.3	13.6	10.3	12.5	9.2
CNF-2	51.0	15.3	11.7	12.2	9.7
CNF-3	41.5	19.1	14.9	14.5	10.0

4.79 nm and 3.43 nm respectively (III). Therefore, compared to other coatings, the surface of the PI coating was smoother. In addition, CNF-3/PI had the lowest roughness compared to CNF/PI, CNF-1/PI and CNF-2/PI, indicating that the increased degree of oxidation had led to the formation of new covalent bonds between the PI resin and the CNFs surface, which was beneficial for the compatibility of the carbon nanofibers with the PI resin[35,38]. In addition, the hardness of the coatings was increased, and the maximum indentation depths of the PI, CNF/PI, CNF-1/PI, CNF-2/PI and CNF-3/PI coatings were 2337 nm, 2080 nm, 2051 nm, 2033 nm and 2022 nm, respectively, as shown in Fig. 6. Additionally, the nanoindentation hardness values were 263.16 MPa, 344.36 MPa, 355.26 MPa, 355.87 MPa and 362.95 MPa. Although the addition of oxidized CNFs does not significantly improve the hardness of PI coatings compared to unoxidized CNFs, the incorporation of CNFs does enhance the hardness of PI coatings to a certain extent.

3.3. Friction and wear resistance of CNF/PI coating

Fig. 7(a-h) showed the coefficient of friction (COF) of the coating and the corresponding wear rate. It was easy to see that the 0.5 wt% coating had the lowest COF and wear rate from 0.1 wt% to 0.7 wt% addition. At 0.5 wt%, the COF were 0.3077 (CNF/PI), 0.3059 (CNF-1/PI), 0.2991 (CNF-2/PI), 0.2643 (CNF-3/PI), and the wear rates were 1.43×10^{-15} m^3/N.m (CNF/PI), 1.34×10^{-15} m^3/N.m (CNF-1/PI), 0.87×10^{-15} m^3/N.m (CNF-2/PI), 0.61×10^{-15} m^3/N.m (CNF-3/PI) (Fig. 8). Therefore, the CNF-3/PI coating had the lowest COF and wear rate compared to the remaining three coatings. In addition, the optimum additive amount of CNFs for PI resin was 0.5 wt%, and the friction performance of the coating decreased when the addition amount reached 0.7 wt%. This was due to the addition of too much CNFs could lead to the formation of large agglomerates in the resin, which reduced the density of the resin, thus causing a decrease in friction performance of the coating. In conclusion,

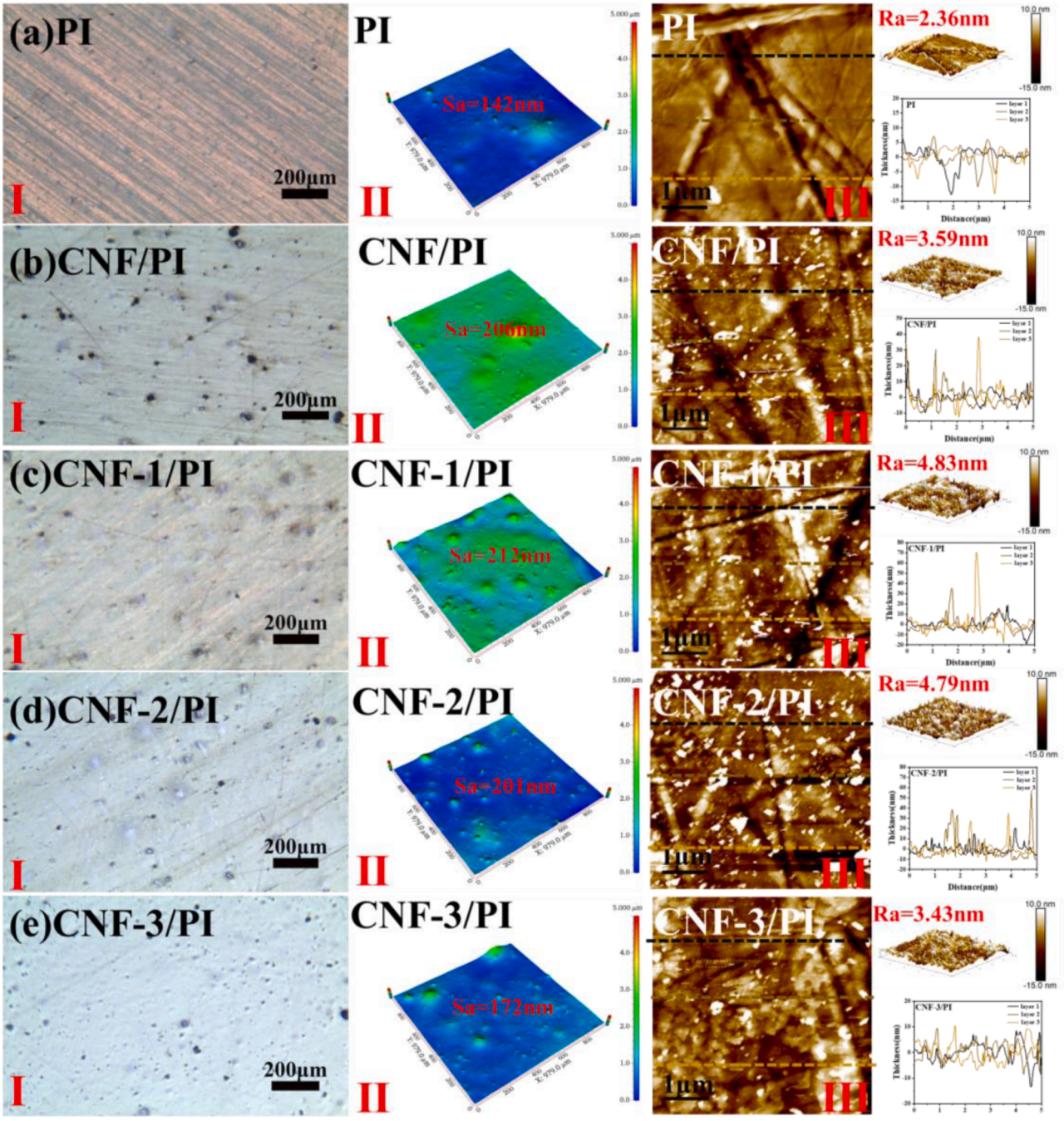

Fig. 5. Optical microscope(I),3D topographies(II) and AFM images, the corresponding 3d diagram and the thickness(III) of the PI(a), CNF/PI(b), CNF-1/PI(c), CNF-2/PI(d) and CNF-3/PI(e).

the introduction of more oxygen-containing functional groups on the surface of CNFs could enhance their compatibility and stability with the resin, thus improving the friction performance of the coating.

Fig.9 showed that to further investigate the improvement of the wear resistance of the PI coating by CNF-3, we observed the morphology of the wear balls after the pure PI, CNF/PI, and CNF-3/PI coatings were worn. White light microscopy showed that the size of the abrasion marks gradually decreased from pure PI to CNF-3/PI, and the scratches on CNF-3/PI were narrower and shallower (I). Measurements of the surface profile using a 3D profilometer further confirmed this result: the surface profile curve of the CNF-3/PI grinding ball was also smoother (II). Therefore, the addition of CNF-3 can effectively improve the wear resistance of PI.

Fig. 10 showed the wear trace morphology of PI, CNF/PI and CNF-3/PI coatings. From the observation of the abrasion mark morphology by optical micrographs, 3D morphology and cross-section profile curves (I, II), the unevenness of the abrasion mark edges of the PI coatings and the bumps at the edge of the abrasion marks indicated that plastic deformation was generated during the friction process. In addition, a plough furrow morphology was visible inside the CNF/PI abrasion marks parallel to the direction of the abrasion marks, exhibiting abrasive wear characteristics. Compared with PI and CNF/PI coatings, CNF-3/PI had significantly narrower and shallower abrasion marks and smoother abrasion cross-section profile curves. Combined with SEM analysis (III, IV), the PI coating wear marks had large spalling pits inside them producing fatigue wear, hence their wear rate was high. With the addition

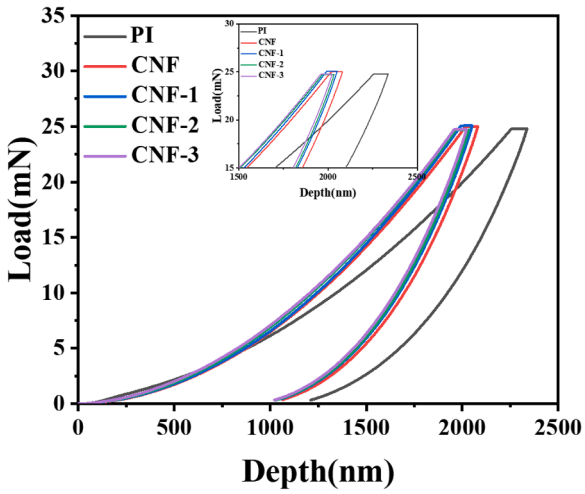

Fig. 6. Hardness of PI, CNF/PI, CNF-1/PI, CNF-2/PI and CNF-3/PI.

of CNFs and CNF-3, the chance of coating flaking due to friction was reduced, and wear was significantly reduced, thus exhibiting a low wear rate. As a result, the oxidized CNF-3 and PI molecular chains fully contact and entangle at the interface, greatly improving the compatibility between the two, thereby densifying the interface area, preventing the generation and propagation of cracks during friction, and improving the wear resistance of the coating.

The abrasive chip morphology of the PI, CNF/PI and CNF-3/PI coatings were further investigated in Fig. 11. The PI coating and CNF/PI coating abrasive chips showed laminated flakes and irregular edges (Fig. 11a-b). The length of the abrasive chips was about 18.67 μm and 9.95 μm, and there were obvious cracks on the surface. The abrasive chips of CNF-3/PI coating showed granular shape and smoother edges (Fig. 11c). The length of the abrasive chips was about 5.23 μm. It indicated that CNF-3 was uniformly dispersed in PI, resulting in a denser coating with a more homogeneous structure. The stress distribution was uniform during the friction process, producing smaller and smooth abrasive chips.

3.4. Corrosion resistance of CNF/PI coatings

The corrosion properties of coatings were further investigated in

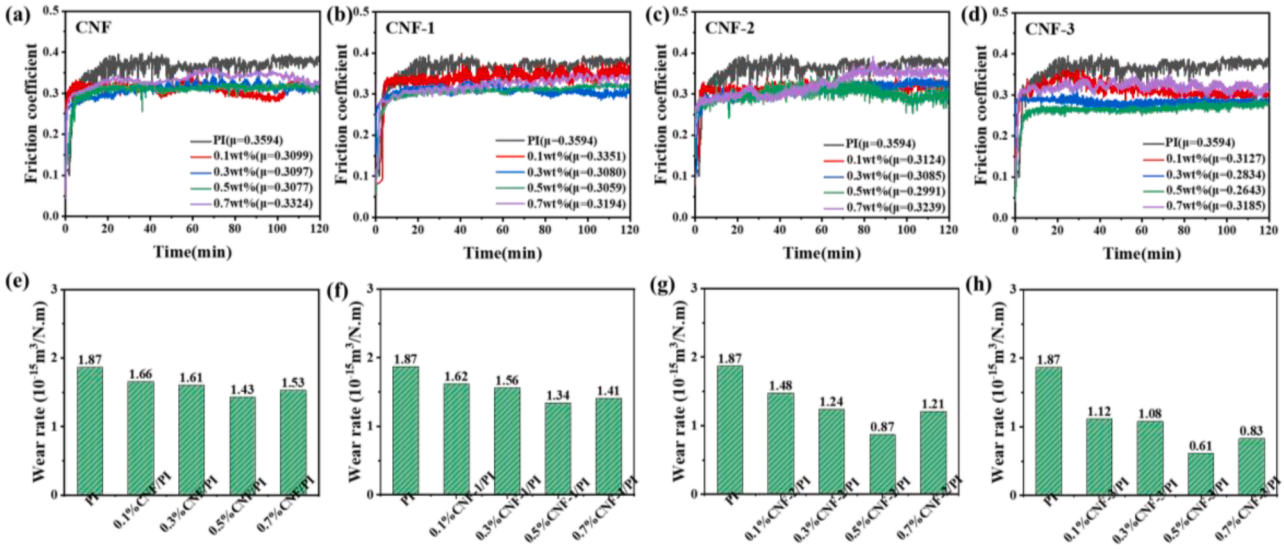

Fig. 7. (a-h) Friction curve and wear rate of the PI, CNF/PI, CNF-1/PI, CNF-2/PI and CNF-3/PI.

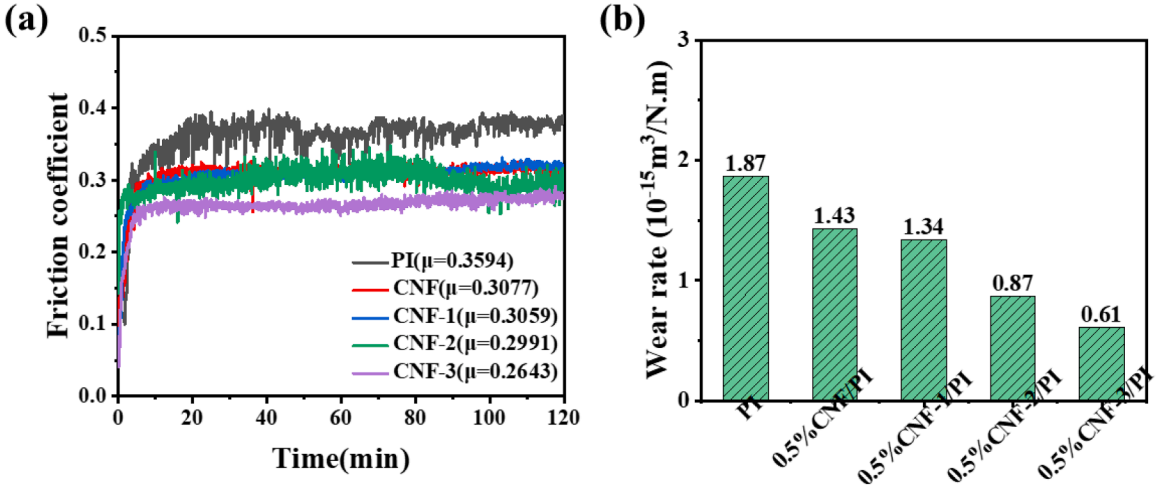

Fig. 8. (a-b) Friction curve and wear rate of the PI, CNF/PI, CNF-1/PI, CNF-2/PI and CNF-3/PI (0.5wt%).

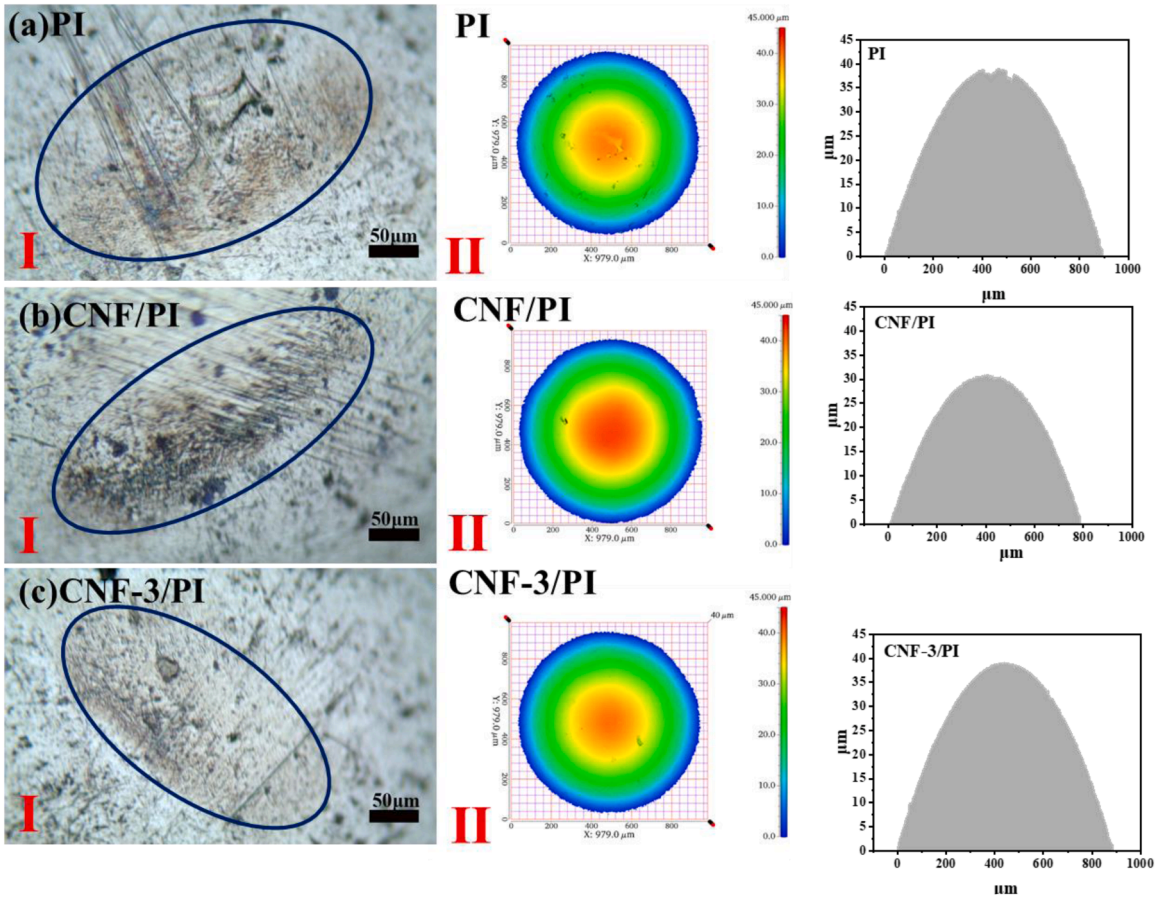

Fig. 9. Grinding ball morphology of the PI(a), CNF/PI(b) and CNF-3/PI (c) optical microscope(I), 3D topographies(II) and the corresponding outline drawing.

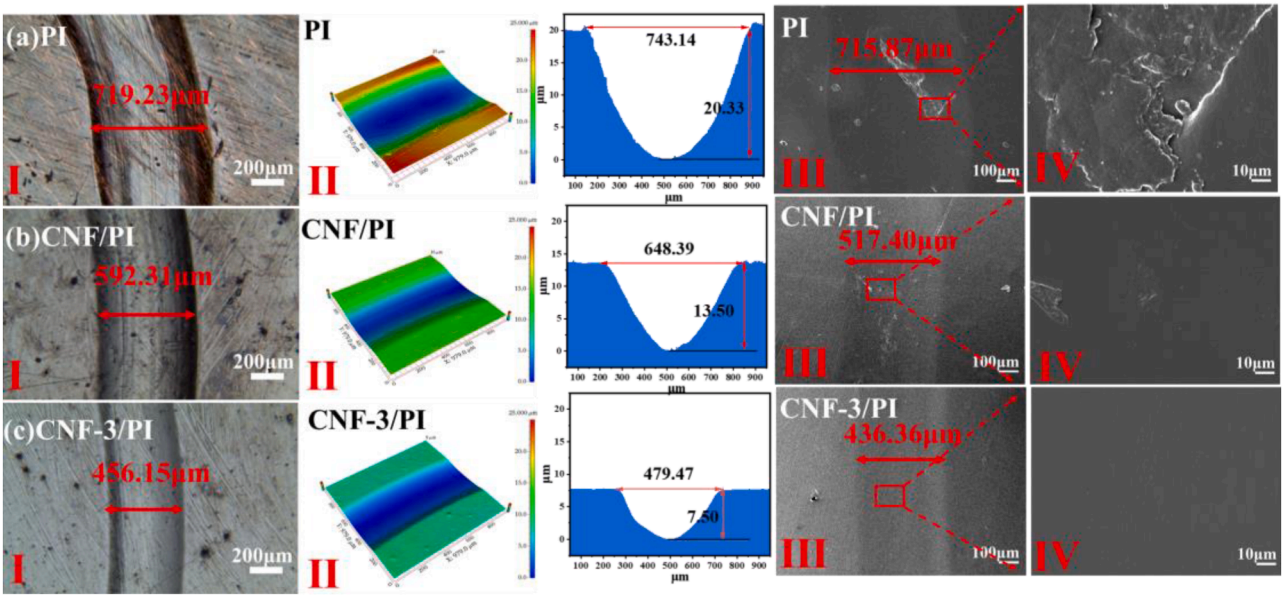

Fig. 10. Wear mark morphology of the PI(a), CNF/PI(b) and CNF-3/PI(c) optical microscope(I), 3D topographies(II) and the corresponding outline drawing and SEM images (III, IV).

Fig. 12. Based on the polarization curves, the E_{corr} of PI, CNF/PI, CNF-1/PI, CNF-2/PI and CNF-3/PI coatings were -0.537 V, -0.575 V, -0.566 V, -0.628 V and -0.545 V. The I_{corr} were 4.0×10^{-7} A/cm^2, 9.0×10^{-7} A/cm^2, 7.5×10^{-7} A/cm^2, 5.9×10^{-7} A/cm^2 and 2.8×10^{-7} A/cm^2. The PI coating had the highest E_{corr}, followed by the CNF-3/PI coating. CNF-3/PI coatings had the lowest I_{corr}. Based on this, there are two main effects of different oxidation levels of CNFs on the corrosion resistance of coatings: firstly, the introduction of oxygen-containing functional groups increases the hydrophilicity of the coatings, resulting in lower E_{corr} for the CNF/PI, CNF-1/PI, CNF-2/PI and CNF-3/PI coatings

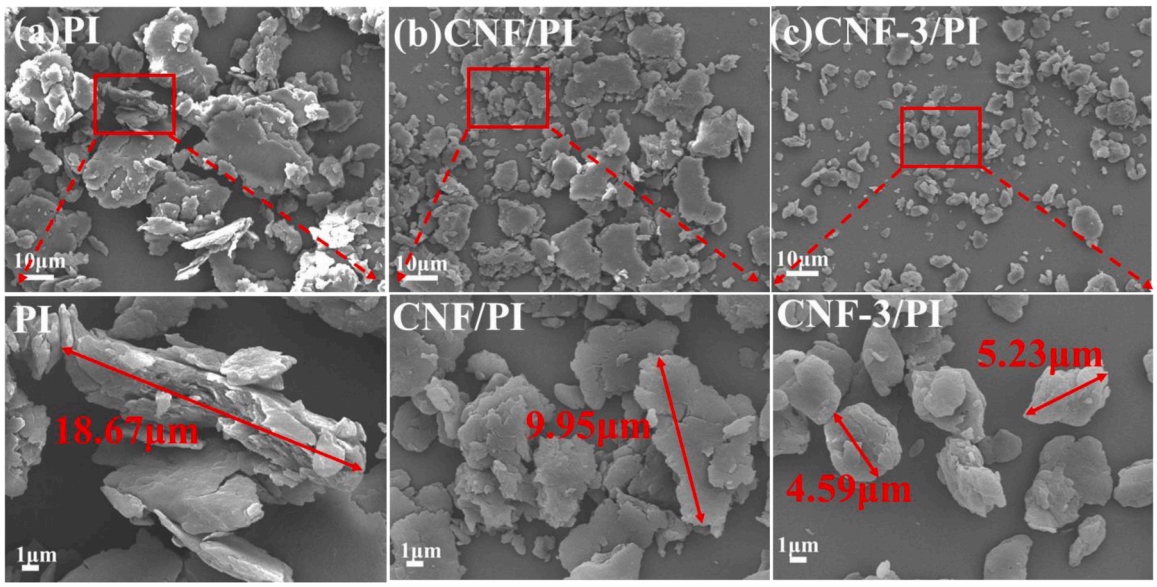

Fig. 11. Morphology of wear debris of the PI, CNF/PI and CNF-3/PI (a-c).

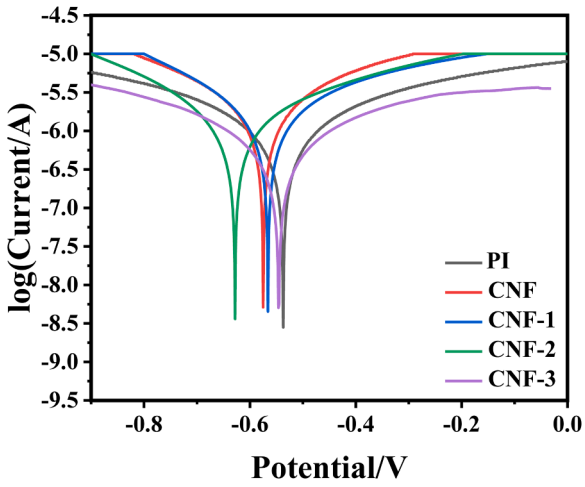

Fig. 12. Polarization curves of PI, CNF/PI, CNF-1/PI, CNF-2/PI and CNF-3/PI coatings.

compared to that of the pure PI coating; secondly, the increase in the degree of oxidation further enhances the dispersion of the nanofillers in the coating as well as the densification of the coating, which slows down the diffusion of corrosive media through the coating, ultimately leading to a reduction in the I_{corr} by 30 %. Fig. 13 further explored the corrosion resistance of the different coatings by observing the post-corrosion morphology of the coatings. It was easy to see that the pure PI coating had the largest corrosion area. In addition, the oxidation of the carbon nanofibers could effectively improve the corrosion resistance of the coatings, as no serious surface corrosion was observed for CNF-1/PI, CNF-2/PI and CNF-3/PI coatings in comparison to CNF/PI coatings.

3.5. *Mechanisms affecting corrosion resistance of CNF*

According to the above studies, both CNF and oxidized CNF can improve the friction and wear properties of PI coating, but their effects on the corrosion resistance are quite different. Thus, in this part, MD simulation was used to investigate the effect mechanism of CNF and oxidized CNF on the corrosion resistance of PI resin.

Fig. 14(a-b) showed the structures of CNF/PI and oxidized CNF/PI after NVT equilibrium. It was worth noting that the compatibility between CNF and oxidized CNF and PI resin differs greatly. Among them, the CNF was farther away from the PI chains, and there no obvious wrapping between them, indicating that CNF was less compatible with the resin. On the other hand, more PI chains were distributed around the oxidized CNF, and a considerable part of PI chains were entangled on the surface of CNF, indicating that the oxidative modification could enhance the compatibility between CNF and PI resin.

Further, the PI, CNF/PI and oxidized CNF/PI were enriched on the Fe substrate. As shown in Fig. 14(c-e), PI, CNF and oxidized CNF all exhibited a clear tendency to aggregate toward the Fe surface, implying that both PI chains and CNF bound well to the Fe substrate. CNFs

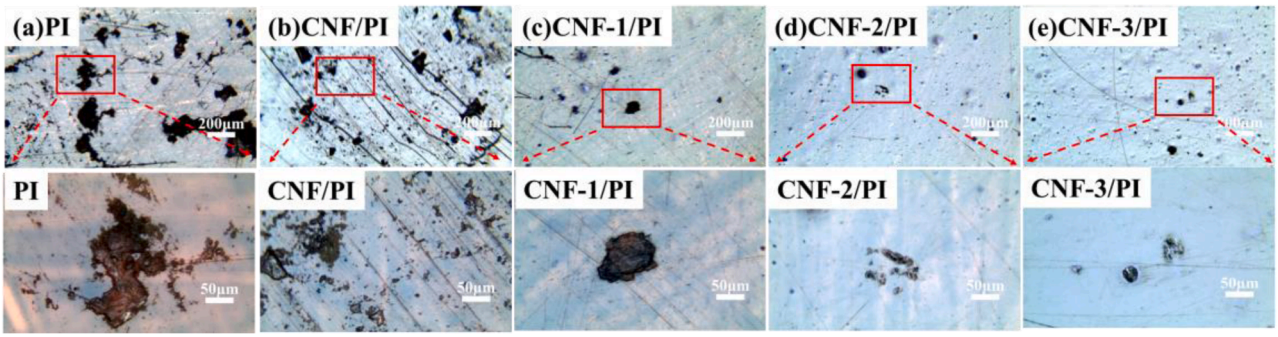

Fig. 13. Morphology of PI, CNF/PI, CNF-1/PI, CNF-2/PI and CNF-3/PI coatings after corrosion (a-e).

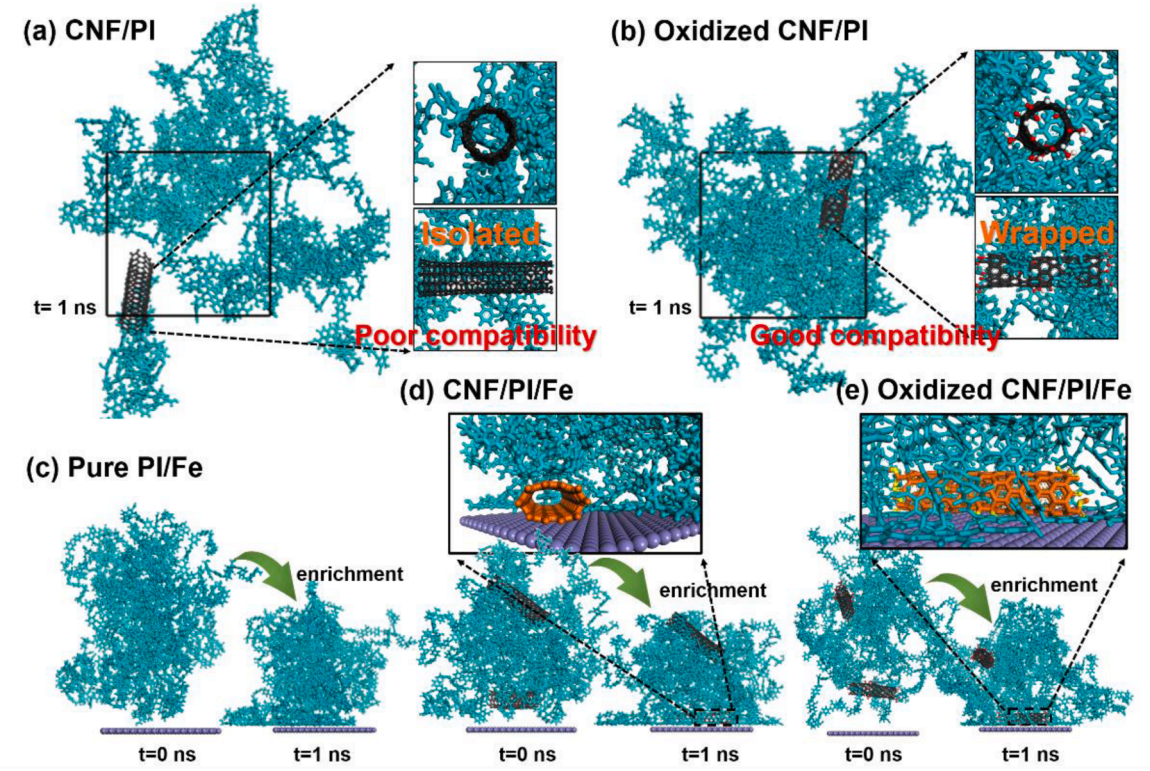

Fig. 14. (a-b) Molecular structures of CNF/PI and oxidized CNF/PI (t=1 ns); (c-e) Enrichment states of PI, CNF/PI and CNF/PI on Fe surface.

underwent some deformation during the enrichment process, but their poor resin compatibility remained unimproved. Oxidized CNFs bound more strongly to the Fe surface and were surrounded by PI chains, which improved the bonding between the PI resin and the Fe substrate.

NaCl-H_2O was constructed on the top of PI, CNF/PI and oxidized CNF/PI to investigate the diffusion of H_2O and Cl^- in different coatings.

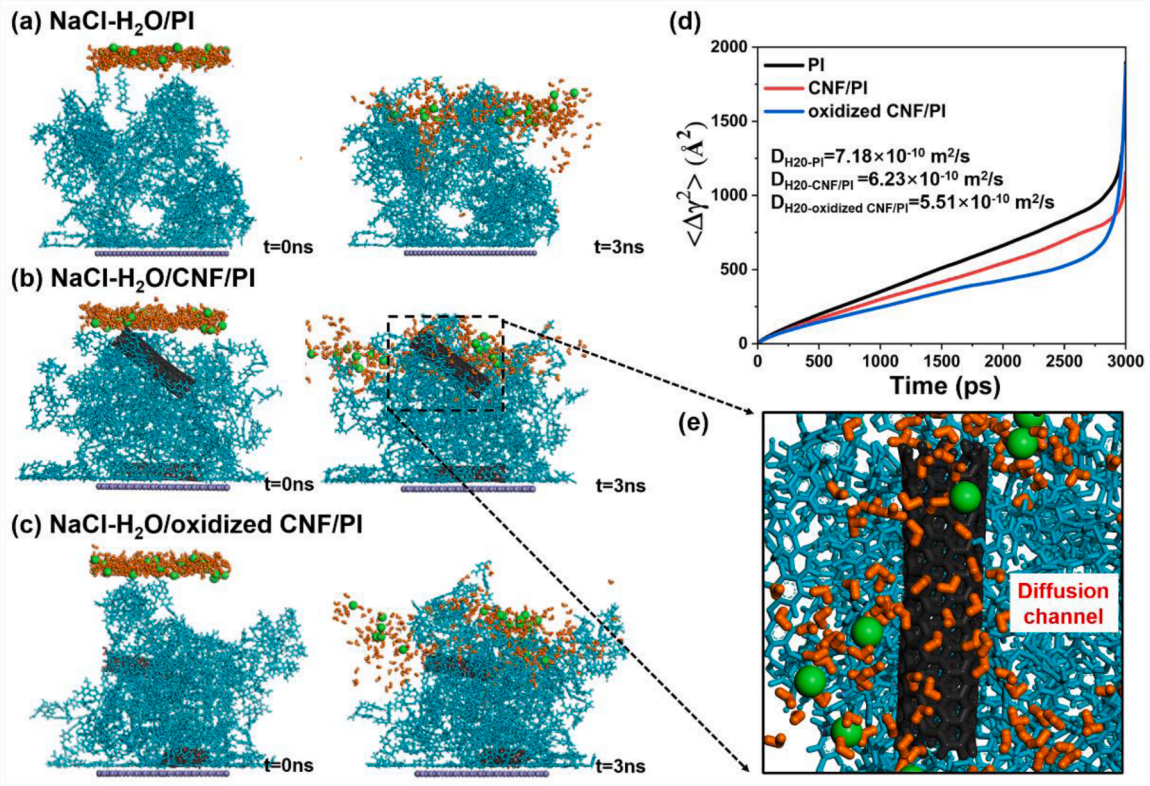

Fig. 15. (a-c) Structure of NaCl-H_2O/PI, NaCl-H_2O/CNF/PI and NaCl-H_2O/oxidized CNF/PI at 0 ns and 3 ns. (d) MSDs of H_2O in NaCl-H_2O/PI, NaCl-H_2O/CNF/PI and NaCl-H_2O/oxidized CNF/PI. (e) Diffusion channel role of CNF.

The simulated structures of the NaCl-H_2O/PI, NaCl-H_2O/CNF/PI and NaCl-H_2O/oxidized CNF/PI at 0 ns and 3 ns were shown in Fig. 15(a-c). For PI coating, the polymer chains were not well aligned and some H_2O and Cl^- diffuse downward along the pores between the PI chains. As for CNF/PI and oxidized CNF/PI, the presence of CNF and oxidized CNF did hinder the diffusion of H_2O and Cl^-. Correspondingly, the diffusion coefficients of H_2O in PI, CNF/PI and oxidized CNF/PI coatings were 7.18×10^{-10} m^2/s, 6.23×10^{-10} m^2/s and 5.51×10^{-10} m^2/s (Fig. 15d) [39,40]. The hindering effect of oxidized CNF was significantly stronger than that of CNF. Moreover, oxidized CNF and PI chains had good compatibility, and the PI chains around the oxidized CNF could form a denser structure, which was conducive to hindering the diffusion of corrosive factors, so that oxidized CNF improved the corrosion resistance of PI resin. However, for CNF/PI coating, due to the poor compatibility between CNF and PI, there are obvious pores at the contact interface, and corrosion factors diffuse along the interface pores, especially in the vertical direction of CNF, resulting in a higher diffusion rate of corrosion factors than that of CNF-3/PI coating, thereby reducing corrosion resistance. Therefore, the compatibility between CNF and PI resin was essential to improve the corrosion resistance.

4. Conclusion

CNF-1 (4 kHz), CNF-2 (20 kHz) and CNF-3 (40 kHz) with different degrees of oxidation were prepared according to the modified Hummers method. The effect of its incorporation into polyimide on the tribological properties as well as the corrosion resistance of polyimide was investigated. The paper draws the following conclusions:

1. CNF-1 (4 kHz), CNF-2 (20 kHz) and CNF-3 (40 kHz) with three different oxidation levels were prepared by controlling the different ultrasound frequencies, the oxygen content was 56.68 %, 57.51 % and 60.72 %.
2. CNF-3/PI (0.5 wt%) achieved the lowest COF (0.2643) and wear rate (0.61×10^{-15} m^3/N.m), which may be due to the introduction of oxygen-containing functional groups that can form new covalent bonds with the PI chains, which not only reduces the agglomeration of CNFs, but also improves the densification and hardness of the coating.
3. Compared with CNFs, CNF-1 and CNF-2, only CNF-3 was favorable for improving the corrosion resistance of the PI coating, with I_{corr} reached a minimum of 2.8×10^{-7} A/cm^2 and E_{corr} raised to -0.545V, indicating that the addition of fillers to corrosion-resistant coatings needs to be very careful.
4. MD simulation results show that both CNF and oxidized CNF hinder the diffusion of corrosion factors to a certain extent, but oxidized CNF has a better bonding force with the resin and a wider range of hindrance. In addition, due to the poor binding force between CNF and PI, pores will be formed on the contact surface, and if the CNF is arranged vertically, the corrosion factor will reach the substrate directly along the pores, resulting in the failure of corrosion resistance.

Therefore, the degree of oxidation of CNFs plays a crucial role in their reinforcement properties. A higher degree of oxidation can significantly enhance the interfacial bonding strength and compatibility between CNFs and the PI matrix. Optimizing this interface is a key prerequisite for enhancing the wear and corrosion resistance of composite materials. The improvement in wear resistance results from efficient stress transfer and energy dissipation enabled by the strong interface, thereby suppressing crack formation and material spalling. Meanwhile, the enhanced corrosion resistance is attributed to the improved dispersion and adhesion of CNFs within the PI matrix, effectively blocking the penetration pathways of corrosive media.

CRediT authorship contribution statement

Huiping Qi: Writing – original draft, Formal analysis, Investigation, Writing – review & editing. **Rui Yuan:** Supervision, Software, Funding acquisition, Conceptualization, Project administration, Writing – review & editing. **Chang Tu:** Formal analysis, Validation. **Hailian Bao:** Resources. **Zhaoyi Zhu:** Data curation. **Zhili Chen:** Data curation. **Jing Yuan:** Funding acquisition, Project administration, Supervision.

Declaration of competing interest

The authors declare that they have no known competing financial interests or personal relationships that could have appeared to influence the work reported in this paper.

Acknowledgments

This work is financially supported by National Natural Science Foundation of China (No. 52265027); Natural Science Foundation of Qinghai province (No. 2024-ZJ-794); Open Project of Salt Lake Chemical Engineering Research Complex, Qinghai University (No. 2023-DXSSZZ-Z03).

Data availability

Data will be made available on request.

References

[1] Y. Tao, F. Ma, M. Teng, Z. Jia, Z. Zeng, Designed fabrication of super high hardness Ni-B-Sc nanocomposite coating for anti-wear application, Appl. Surf. Sci. 492 (2019) 426–434, https://doi.org/10.1016/j.apsusc.2019.06.233.
[2] H. Liu, B. Yang, C. Wang, Y. Han, D. Liu, The mechanisms and applications of friction energy dissipation, Friction 11 (2022) 839–864, https://doi.org/10.1007/s40544-022-0639-0.
[3] W. Chen, W. Wang, P. Zhu, X. Ge, Effects of pore size on the lubrication properties of porous polyimide retainer material, Friction 11 (2023) 1419–1429, https://doi.org/10.1007/s40544-022-0670-1.
[4] C. Yang, P. Jiang, H. Qin, X. Wang, Q. Wang, 3D printing of porous polyimide for high-performance oil impregnated self-lubricating, Tribol. Int. (2021) 160, https://doi.org/10.1016/j.triboint.2021.107009.
[5] R.L. Fusaro, H.E. Sliney, Lubricating characteristics of polyimide bonded graphite fluoride and polyimide thin films, ASLE Trans. 16 (1973) 189–196, https://doi.org/10.1080/05698197308982721.
[6] H. Yuan, S. Yang, X. Liu, Z. Wang, L. Ma, K. Hou, Z. Yang, J. Wang, Polyimide-based lubricating coatings synergistically enhanced by MoS_2@HCNF hybrid, Compos. A Appl. Sci. Manuf. 102 (2017) 9–17, https://doi.org/10.1016/j.compositesa.2017.07.013.
[7] L. Mu, J. Zhu, J. Fan, Z. Zhou, Y. Shi, X. Feng, H. Wang, X. Lu, M. Amaral, Self-lubricating polytetrafluoroethylene/polyimide blends reinforced with zinc oxide nanoparticles, J. Nanomater. 2015 (2015), https://doi.org/10.1155/2015/545307.
[8] A. Roy, L. Mu, Y. Shi, Tribological properties of polyimide-graphene composite coatings at elevated temperatures, Prog. Org. Coat. (2020) 142, https://doi.org/10.1016/j.porgcoat.2020.105602.
[9] G. Chen, S. Jiang, Y. Huang, X. Wang, C. Chai, Design of ternary solid lubricants SiO2/Ti3C2/PTFE for wear-resistant, self-lubricating polyimide composites, J. Taiwan. Inst. Chem. Eng. (2024) 157, https://doi.org/10.1016/j.jtice.2024.105429.
[10] Y. Cui, C. Liu, S. Hu, X. Yu, The experimental exploration of carbon nanofiber and carbon nanotube additives on thermal behavior of phase change materials, Sol. Energy Mater. Sol. Cells 95 (2011) 1208–1212, https://doi.org/10.1016/j.solmat.2011.01.021.
[11] A. Elgafy, K. Lafdi, Effect of carbon nanofiber additives on thermal behavior of phase change materials, Carbon. N. Y. 43 (2005) 3067–3074, https://doi.org/10.1016/j.carbon.2005.06.042.
[12] J.C. Ruiz-Cornejo, D. Sebastián, M.J. Lázaro, Synthesis and applications of carbon nanofibers: a review, Rev. Chem. Eng. 36 (2020) 493–511, https://doi.org/10.1515/revce-2018-0021.
[13] M.H. Cho, S. Bahadur, Study of the tribological synergistic effects in nano CuO-filled and fiber-reinforced polyphenylene sulfide composites, Wear 258 (2005) 835–845, https://doi.org/10.1016/j.wear.2004.09.055.
[14] Y. Wu, Y. He, C. Chen, H. Li, Y. Xia, T. Zhou, MoS_2-CNFs composites to enhance the anticorrosive and mechanical performance of epoxy coating, Prog. Org. Coat. 129 (2019) 178–186, https://doi.org/10.1016/j.porgcoat.2019.01.021.
[15] J. Zhu, L. Mu, L. Chen, Y. Shi, H. Wang, X. Feng, X. Lu, Interface-strengthened polyimide/carbon nanofibers nanocomposites with superior mechanical and

tribological properties, Macromol. Chem. Phys. 215 (2014) 1407–1414, https://doi.org/10.1002/macp.201400194.
[16] A.R. Siddiqui, R. Maurya, P.K. Katiyar, K. Balani, Superhydrophobic, self-cleaning carbon nanofiber CVD coating for corrosion protection of AISI 1020 steel and AZ31 magnesium alloys, Surf. Coat. Tech. 404 (2020), https://doi.org/10.1016/j.surfcoat.2020.126421.
[17] F. Bensalah, J. Pézard, N. Haddour, M. Erouel, F. Buret, K. Khirouni, Carbon nanoFiber/PDMS composite used as corrosion-resistant coating for copper anodes in microbial fuel cells, Nanomaterials (2021) 11, https://doi.org/10.3390/nano11113144.
[18] Y. Zhao, M. Huang, Z. Gao, H. He, Y. Chen, F. He, Y. Lin, B. Yan, S. Chen, Preparation of polyaniline/cellulose nanofiber composites with enhanced anticorrosion performance for waterborne epoxy resin coatings, Polym. Eng. Sci. 63 (2023) 1613–1622, https://doi.org/10.1002/pen.26310.
[19] A.G. Bannov, V.K. Varentsov, I.S. Chukanov, E.V. Gorodilova, G.G. Kuvshinov, Comparative analysis of methods of oxidative modification of carbon nanofibers, Prot. Met. Phys. Chem. 48 (2012) 199–206, https://doi.org/10.1134/s2070205112020037.
[20] Y. Nie, T. Hübert, Surface modification of carbon nanofibers by glycidoxysilane for altering the conductive and mechanical properties of epoxy composites, Compos. Part a Appl. Sci. Manuf. 43 (2012) 1357–1364, https://doi.org/10.1016/j.compositesa.2012.03.025.
[21] P.-y. Hung, K.-t. Lau, B. Fox, N. Hameed, J.H. Lee, D. Hui, Surface modification of carbon fibre using graphene–related materials for multifunctional composites, Compos. B Eng. 133 (2018) 240–257, https://doi.org/10.1016/j.compositesb.2017.09.010.
[22] Z. Cai, X. Meng, X. Zhang, L. Cui, Q. Zhou, Effects of surface modification of carbon nanofibers on the mechanical properties of polyamide 1212 composites, J. Appl. Polym. Sci. (2014) 132, https://doi.org/10.1002/app.41424.
[23] A. Rasheed, J.Y. Howe, M.D. Dadmun, P.F. Britt, The efficiency of the oxidation of carbon nanofibers with various oxidizing agents, Carbon. N. Y. 45 (2007) 1072–1080, https://doi.org/10.1016/j.carbon.2006.12.010.
[24] L. Calvillo, M.J. Lázaro, I. Suelves, Y. Echegoyen, E.G. Bordejé, R. Moliner, Study of the surface chemistry of modified carbon nanofibers by oxidation treatments in liquid phase, J. Nanosci. Nanotechnol. 9 (2009) 4164–4169, https://doi.org/10.1166/jnn.2009.M26.
[25] M. Moradi, M. Rezaei, Long-term experimental evaluation and molecular dynamics simulation of polypropylene/graphene oxide nanocomposite coating in 3.5 wt% NaCl solution, Prog. Org. Coat. (2022) 164, https://doi.org/10.1016/j.porgcoat.2022.106718.
[26] C. Tu, R. Yuan, H. Qi, L. Chen, X. Qin, J. Yuan, Does the dispersion method affect the tribological properties of graphene oxide? Surf. Coat. Tech. (2025) 497, https://doi.org/10.1016/j.surfcoat.2025.131737.
[27] T. Lou, X. Bai, X. He, Y. Yang, C. Yuan, Molecular dynamics simulation of peptide attachment on Al-based surfaces, Prog. Org. Coat. (2021) 157, https://doi.org/10.1016/j.porgcoat.2021.106310.
[28] R. Yuan, L. Gao, J. Liu, C. Tu, R. Tan, S. Xu, Effect of hydrophobic alkyl chains on the plasticization properties of citrate: Experiments and MD simulation, Eur. Polym. J. (2024) 203, https://doi.org/10.1016/j.eurpolymj.2023.112644.
[29] R. Yuan, P. Li, L. Chen, J. Yuan, B. Xu, G. Sun, E. Ding, J. Chen, Effects of grafting oxygen atoms on the tribological properties of graphene: Molecular dynamics simulation and experimental analysis, Appl. Surf. Sci. (2020) 528, https://doi.org/10.1016/j.apsusc.2020.147045.
[30] M.A. Ermakova, D.Y. Ermakov, V.V. Kaichev, G.G. Kuvshinov, Chemical properties of the surface of nanofibrous carbonaceous materials produced by catalytic methane decomposition, Russ. J. Phys. Chem. 80 (2006) 886–891, https://doi.org/10.1134/s0036024406060082.
[31] I. Ud Din, M.S. Shaharun, D. Subbarao, A. Naeem, Surface modification of carbon nanofibers by HNO_3 treatment, Ceram. Int. 42 (2016) 966–970, https://doi.org/10.1016/j.ceramint.2015.08.054.
[32] R.-S. Zhong, Y.-H. Qin, D.-F. Niu, J.-W. Tian, X.-S. Zhang, X.-G. Zhou, S.-G. Sun, W.-K. Yuan, Effect of carbon nanofiber surface functional groups on oxygen reduction in alkaline solution, J. Power. Sources. 225 (2013) 192–199, https://doi.org/10.1016/j.jpowsour.2012.10.043.
[33] T.G. Ros, A.J. van Dillen, J.W. Geus, D.C. Koningsberger, Surface oxidation of carbon nanofibres, Chem. Eur. J. 8 (2002) 1151–1162, https://doi.org/10.1002/1521-3765(20020301)8:5<1151::Aid-chem1151>3.0.Co;2-#.
[34] T. Ramanathan, F.T. Fisher, R.S. Ruoff, L.C. Brinson, Amino-functionalized carbon nanotubes for binding to polymers and biological systems, Chem. Mater. 17 (2005) 1290–1295, https://doi.org/10.1021/cm048357f.
[35] Y. Nie, Surface silanization of carbon nanofibers and nanotubes for altering the properties of epoxy composites, (2012).
[36] S.E. Moosavifard, J. Shamsi, S. Fani, S. Kadkhodazade, Facile synthesis of hierarchical CuO nanorod arrays on carbon nanofibers for high-performance supercapacitors, Ceram. Int. 40 (2014) 15973–15979, https://doi.org/10.1016/j.ceramint.2014.07.126.
[37] W. Li, R. Bi, G. Liu, Y. Tian, L. Zhang, 3D Interconnected MoS_2 with enlarged interlayer spacing grown on carbon nanofibers as a flexible anode toward superior sodium-ion batteries, ACS. Appl. Mater. Interfaces. 10 (2018) 26982–26989, https://doi.org/10.1021/acsami.8b05825.
[38] Z.J. Zhang, X.Y. Chen, Carbon nanofibers derived from bacterial cellulose: Surface modification by polydopamine and the use of ferrous ion as electrolyte additive for collaboratively increasing the supercapacitor performance, Appl. Surf. Sci. (2020) 519, https://doi.org/10.1016/j.apsusc.2020.146252.
[39] S. Bi, T. Zhao, J. Tuo, X. Wang, Y. Sun, Y. Zhang, Physical evolution mechanism of polyimide/fluorinated graphene composite insulating materials under extreme conditions, Prog. Org. Coat. (2025) 200, https://doi.org/10.1016/j.porgcoat.2025.109065.
[40] Z. Zhang, Z. Wu, S. Zheng, H. Yang, F. Tian, Multiscale analysis of breakdown strength in polyimide nanocomposite films: Simulations, experiments, and machine learning, Prog. Org. Coat. (2025) 200, https://doi.org/10.1016/j.porgcoat.2025.109058.